Pyrolysis of Furan in a Microreactor

Kimberly N. Urness,[1] Amir Golan,[2] John W. Daily,[1] Mark R. Nimlos,[3] John F. Stanton,[4] Musahid Ahmed,[2] G. Barney Ellison[5]

[1] Center for Combustion and Environmental Research
Department of Mechanical Engineering
University of Colorado at Boulder
Boulder, CO 80309-0427
Email: john.daily@colorado.edu

[2] Chemical Sciences Division
LBNL MS 6R-2100
Berkeley CA 94720
Email: mahmed@lbl.gov

[3] National Renewable Energy Laboratory
1617 Cole Blvd.
Golden, CO 80401
Email: mark_nimlos@nrel.gov

[4] Institute for Theoretical Chemistry
Department of Chemistry
University of Texas
Austin, TX 78712
Email: jfstanton@mail.utexas.edu

[5] Department of Chemistry and Biochemistry
University of Colorado
Boulder, CO 80309-0215
Email: barney@jila.colorado.edu

[submitted to *J. Chem. Phys.*, March 2013]

Abstract

A silicon carbide microtubular reactor has been used to measure branching ratios in the thermal decomposition of furan, C_4H_4O. The pyrolysis experiments are carried out by passing a dilute mixture of furan (roughly 0.01 %) entrained in a stream of helium through the heated reactor. The SiC reactor (0.6 mm i.d, 2 mm o.d., 2.5 cm long) operates with continuous flow. Experiments were performed with a reactor inlet pressure of 100–300 Torr and a "chemical temperature" within the reactor of approximately 1100–1400 K; characteristic residence times in the reactor are 100–200 μsec. Tunable synchrotron radiation photoionization mass spectrometry is used to monitor the products, measure the branching ratio

of the two carbenes as well as the ratio of [$HCCCH_2$]/[$HC{\equiv}CCH_3$]. The results of our experiments clearly demonstrate a preference for the decomposition channel through a β-carbene. At temperatures of 1100–1200 K, only $HC{\equiv}CCH_3$ is produced. As the temperature rises to 1300–1400 K, roughly 10 % of the flux through the β-carbene channel goes to $HCCCH_2$ radicals.

I. Introduction

Recently chemical engineers[1] and organic chemists[2] have made significant progress in extracting a variety of renewable fuels from lignocellulosic biomass.[3] In particular, a low-temperature non-enzymatic pathway has been developed to produce 2-methylfuran (2MF) and 2,5-dimethylfuran (DMF) from cellulose. DMF is a promising biofuel since it has an energy content[2,4,5] (29.6 kJ cm^{-3} at 298 K) similar to that of gasoline (≅ 32 kJ cm^{-3} at 298 K) and significantly greater than that of ethanol (21.2 kJ cm^{-3} at 298 K). It is likely that there will be other fuels derived from lignocellulosic biomass beyond 2MF and DMF.[3]

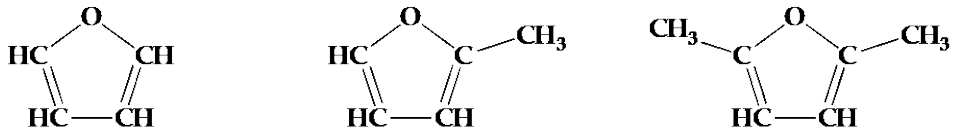

furan m/z 68 | **2-methylfuran** m/z 82 | **2, 5-dimethylfuran** m/z 96 (1)

The furans described above are just the first of several possible new propellants that are proposed as second-generation biofuels. The combustion processes of these complex, oxygen-containing species are of current interest[6,7] and have only recently been subjected to engine studies.[8,9,10] We use a heated microtubular (μtubular) reactor as a device to study the pyrolysis of these new oxygenated fuels. The μtubular reactor[11] operates at a nominal pressure of 100 Torr and at temperatures up to about 1600 K. The goal of this paper is to describe the nature of the pyrolysis of furan, the parent compound in eq. (1).

In earlier studies, the thermal decomposition of furan was studied in flow tubes,[12,13] shock tubes,[14,15,16] and by IR homogeneous pyrolysis.[17] These studies were conducted over a wide range of pressure (1 mTorr – 20 atm) and temperature (500 K – 3000 K). The consensus from these experiments is that the initial step in furan pyrolysis is ring opening to a diradical, "L-C_4H_4O". Subsequent fragmentation of L-C_4H_4O led to the production of alkynes and ketene as the important primary products: furan (+ M) → L-C_4H_4O → CO + HC≡CH + $CH_3C{\equiv}CH$/$CH_2{=}C{=}CH_2$ + $CH_2{=}C{=}O$. In 2000, a computational study[18] predicted that furan pyrolysis followed two separate pathways involving a pair of carbenes, which collectively represent the "L-C_4H_4O" species above. The α-carbene was computed to decompose to HC≡CH + $CH_2{=}C{=}O$ while the β-carbene was predicted to isomerize to allenyl-aldehyde, $CH_2{=}C{=}CH{-}CHO$, which subsequently fragments to $CH_3C{\equiv}CH$ + CO or breaks apart to radicals, H + CO + $HCCCH_2$.

Recently a pulsed SiC μtubular reactor was used to decompose furan.[19] The pyrolysis experiments were carried out by passing a dilute mixture of furan (roughly 0.1 %) entrained in a stream of a buffer gas (either He or Ar) through a SiC reactor that is 2-3 cm long and 1 mm in diameter. The SiC tube wall temperature was in the range 1200–1700 K and the characteristic residence times in the reactor were 100–200 μsec. Products formed at early pyrolysis times in the μtubular reactor were identified by fixed frequency (118.2 nm or 10.487 eV)

photoionization mass spectroscopy (PIMS) as well as matrix-isolation infrared spectroscopy. In addition to [CO, HC≡CH, $CH_3C{\equiv}CH$, $CH_2{=}C{=}O$], clear evidence for the production of propargyl radical, $HCCCH_2$, was found. Based on these experiments,[19] the predicted mechanism[18] for the pyrolysis of furan was verified and is outlined in Scheme I.

We have re-studied the pyrolysis of furan-d_0 and furan-d_4 in a heated μtubular flow reactor over a range of temperatures. The goals of this paper are to use tunable PIMS to again confirm the furan pyrolysis mechanism in Scheme I and also to measure the branching ratio. Scheme I predicts that the observed furan pyrolysis products result from a sequence of unimolecular fragmentations involving carbene intermediates.

$$\text{Furan (+ M)} \rightleftharpoons [\alpha\text{-carbene}] \rightarrow HC{\equiv}CH + CH_2{=}C{=}O \tag{2a}$$

$$\text{Furan (+ M)} \rightleftharpoons [\beta\text{-carbene}] \rightarrow HC{\equiv}C\text{-}CH_3 + CO \tag{2b}$$

$$\text{Furan (+ M)} \rightleftharpoons [\beta\text{-carbene}] \rightarrow H + HCCCH_2 + CO \tag{2c}$$

We measure the branching ratio of the pyrolysis products in eq. (2) as a function of temperature.

$$\left[\frac{\alpha-\text{carbene}}{\beta-\text{carbene}}\right]_T = \frac{[HCCH]}{[CO]} = \frac{[HCCH]}{[HCCCH_2]+[HCCCH_3]} = \frac{[CH_2CO]}{[HCCCH_2]+[HCCCH_3]} = \frac{[CH_2CO]}{[CO]} \tag{3}$$

In addition, the temperature dependence of the ratio of propargyl radicals to methylacetylene is measured

$$\left[\frac{[HCCCH_2]}{[HCCCH_3]}\right]_T \tag{4}$$

II. Measurement of Product Ratios *via* Photoionization

Photoionization has the potential to quantify the composition of a gas mixture. Ionization of a neutral target such as acetylene or furan produces an ion signal, which is proportional to the target concentration in the area sampled by the photon source. The PIMS signal in a dilute gas can be understood by a formulation of Beer's law.[20] For photoionization, the ion signal is a function of the number of molecules in the interaction region, the VUV photon flux through the volume, and the photoionization cross section. However, the absolute value of neither the volume nor the photon flux is known. The volume can be estimated with some uncertainty, however, it can also be gathered into an empirical constant obtained by calibration which ultimately cancels when taking ratios. The photon fluxes are measured using a photodiode. Therefore, to a first approximation, the photoionization signal S_i^+ due to species *i* can be written as:

$$S_i^+ = C\, n_i\, \Phi(E)\, \sigma_i(E) \tag{5}$$

where n_i is the number density of species *i* in the interaction volume, $\Phi(E)$ the photon flux at a given energy, and $\sigma_i(E)$ the energy-dependent molecular photoionization cross section. Here the signal S_i^+ refers to the total ion counts summed over the given mass peak and normalized on the sampling time or number of scans. Expression (5) ignores the fact that because of differential diffusion and other factors, molecules of differing mass and collision cross sections will be detected with different efficiency. This effect is taken into account by defining a mass discrimination factor D_i that is empirically determined by calibration.[21] Incorporating the mass discrimination factor and solving for the number density of the neutral target, one finds:

$$\mathbf{n}_i = \frac{S_i^+}{\mathrm{C}\,\mathrm{D}_i\Phi(\mathrm{E})\sigma_i(\mathrm{E})} \tag{6}$$

The constant C contains all the geometry dependent factors that do not change with differing mass, which could be obtained by absolute calibration.

However, while it would be difficult to use (6) to measure the absolute concentration of a species, it should be straightforward to measure the ratios (3) and (4)

$$\frac{\alpha-\mathrm{Carbene}}{\beta-\mathrm{Carbene}} = \frac{[\mathrm{HCCH}]}{[\mathrm{CO}]} = \frac{S_{26}^+}{S_{28}^+}\left[\frac{\mathrm{D}_{\mathrm{CO}}\Phi_{\mathrm{CO}}\sigma_{\mathrm{CO}}}{\mathrm{D}_{\mathrm{HCCH}}\Phi_{\mathrm{HCCH}}\sigma_{\mathrm{HCCH}}}\right] \tag{7}$$

where the photon flux also cancels if the same photon energy is used to measure both species. Similarly, the ratio of propargyl radicals to methylacetylene becomes:

$$\frac{[\mathrm{HCCCH_2}]}{[\mathrm{HCC\text{-}CH_3}]} = \frac{S_{39}^{+}}{S_{40}^{+}} \left[\frac{D_{\mathrm{HCC\text{-}CH_3}} \Phi_{\mathrm{HCC\text{-}CH_3}} \sigma_{\mathrm{HCC\text{-}CH_3}}}{D_{\mathrm{HCCCH_2}} \Phi_{\mathrm{HCCCH_2}} \sigma_{\mathrm{HCCCH_2}}} \right] \tag{8}$$

with the same caveat regarding the ratio of photon fluxes. The ionization energies of carbon monoxide,[22] acetylene,[23] propargyl radical,[24] methylacetylene,[25] ketene,[26] and furan[27] are known. To measure the ratios *via* (7) and (8) requires knowledge of the photoionization cross sections of these species.[21,28,29,30,31] The mass discrimination factors, D_i, can be estimated by calibration. A calibrated gas mixture containing known quantities of H_2, Ar, Kr, and Xe was sampled by PIMS and the ion counts recorded; the best fit for D_i in eq. (6) was $(m_i)^{0.51\pm0.11}$. For these experiments, it was found that D_i is roughly proportional to the square root of the mass, which is the scaling behavior of average molecular speeds in the Maxwell-Boltzmann distribution. A similar approach to estimating mass discrimination factors was reported earlier. [32]

A careful measurement of the ratios (3) and (4) represents a first step to quantify the initial pyrolysis steps of the aromatic oxygenated fuel, furan.

III. Experimental

Experiments were performed at Lawrence Berkeley National Laboratory's Advanced Light Source (ALS) using a continuous flow (CW) μtubular reactor and time-of-flight photoionization mass spectrometry (PIMS) to identify the mass to charge ratio (m/z) of the molecular species at the reactor exit. A similar version of the reactor was described in detail in a recent publication.[11] For the experiments presented in this work, the reactor is a silicon carbide (SiC) tube (0.6 mm i.d, 2 mm o.d., 2.5 cm long), mounted to a standard stainless steel Swagelok fitting (1/8″ to 3/8″ reducing union) and secured with a graphite ferrule (Restek, 1/8″ tube, inner diameter drilled out to fit reactor). For all experiments, the mass flow rate was held constant at 280 sccm He with a commercial mass flow controller (MKS P4B 0-200 sccm N_2). The pressure upstream of the reactor was measured with a capacitance monometer pressure gauge. Since the mass flow rate was held constant, the upstream pressure increases with the temperature of the SiC wall due to the larger frictional effects in the flow. With the reactor at room temperature, the upstream pressure was about 100 Torr. Increasing the measured SiC wall temperature to 1600 K increased the upstream pressure to about 300 Torr. The reactor exhausts into a chamber at a pressure of 10 μTorr. The pressure profile inside the reactor monotonically decreases along the 2.5 cm length of the reactor. With a measured wall temperature of 1600 K the pressure profile along the centerline has been estimated by computational fluid dynamics to decrease from about 300 Torr at the entrance to 50 Torr at the exit.[33] Approximately 2 cm of the SiC is resistively heated, with the temperature of the

outer wall measured with a Type C thermocouple[34] and also monitored with an infrared thermometer (Omega iR2P temperature controller, range 600˚C to 1600˚C). Reactant mixtures were made in stainless steel cylinders with concentrations between 0.0075% and 0.15% furan (Sigma Aldrich, ≥ 99%) in helium (final tank pressure between 3 to 6.5 atm).

The μtubular reactor used for these experiments is not very well characterized. Because the reactor is very small, a few centimeters in length and 0.5–1 mm in inner diameter, it is not possible to either insert sampling probes or readily gain optical access as would be the case for a larger scale reactor or a shock tube. This has limited our experimental ability to measure only flow boundary conditions and wall temperature, as well as to analyze the product composition.

Given the limited physical access, simulation is the best way to characterize the flow field. Computational fluid dynamics should be able to simulate conditions in these small microreactors. However, since the reactor exhausts into a 10^{-5} Torr vacuum chamber (as is required for matrix isolation and photoionization mass spectrometry diagnostics) the local Knudsen number changes from continuum conditions to rarefied flow within the reactor. As a result, a proper simulation requires a coupled continuum/particle approach to which we are currently working toward a solution.[33]

The rates of chemical reactions in these μtubular reactors are of course very sensitive to temperature and there will be a distribution of temperatures

across the tube. Gases at the wall are hotter than those along the centerline of the reactor. In order to characterize an approximate temperature in the reactor, preliminary experiments have been carried out[35] using cyclohexene as a "chemical thermometer".[36] Cyclohexene was thermally decomposed: cyclohexene (+ M) $\rightarrow$ ethylene + 1,3-butadiene and the extent of cyclohexene decomposition was monitored *via* PIMS with tunable VUV light from the synchrotron at LBNL's Advanced Light Source. Although the data analysis is somewhat complicated by dissociative ionization of cyclohexene, these measurements were analyzed to yield $T_{chemical}$ of 1200 – 1250 K with a measured SiC wall temperature of 1400 K. However, a chemical thermometer will only give an average, kinetically weighted temperature. Thus, the effective "chemical temperature" in the reactor is somewhat below the wall temperature. Based on this preliminary result the effective temperatures in the 1000–1400K range reported here correspond to the measured wall temperature minus 200 K. Further experiments and a reactive computational fluid dynamics modeling effort are underway.[33]

The molecular beam is interrogated by synchrotron radiation about 10 cm downstream from the skimmer. The ions were detected using a microchannel plate and the signal was recorded by ion counting. Most experiments reported here involved 100,000 sweeps at each photon energy. Photoionization efficiency (PIE) curves for a given mass to charge ratio (m/z) were obtained by plotting the summation of the background corrected ion signal in an appropriate mass range

versus the selected photon energy, normalized by the photon flux as measured by a photodiode with a calibrated energy dependent efficiency.

IV. Results

a) Confirmation of Furan Pyrolysis Mechanism in Scheme I

The mechanism for furan pyrolysis in Scheme I is based on experiments[19] with a pulsed SiC μtubular reactor with fixed frequency PIMS and IR detection. Fig. 1 plots the PIMS that result from the thermal cracking of furan in helium in a CW SiC μtubular reactor with tunable VUV radiation. VUV (11.0 eV) PIMS of furan, diluted to 0.15% in He, was heated to an estimated effective chemical temperature of 1400 K (a measured wall temperature of 1600 K, as described in Section III) and produced ions at m/z 15, 39, 40, 42, 50, 52, 68, and 78. Scheme I predicts furan (m/z 68), ketene (m/z 42), methylacetylene (m/z 40), and propargyl radical (m/z 39). The H atoms, acetylene, and carbon monoxide predicted by the mechanism will not be ionized by 11.0 eV photons. The PIMS on the left hand side of Fig. 1 clearly shows the presence of CH_3 radicals[37] (m/z 15) which are not consistent with Scheme I. One possible source of methyl radicals could be bimolecular chemistry triggered by H atoms. Reaction of H atoms produced by Scheme I with methylacetylene might produce methyl radicals as well as allene.

$$H + CH_3\text{-}C{\equiv}C\text{-}H \rightleftharpoons [CH_3CH{=}CH]^* \rightarrow CH_3 + HC{\equiv}CH \qquad (9a)$$

$$\rightleftharpoons [CH_3C{=}CH_2]^* \rightarrow H + CH_2{=}C{=}CH_2 \quad (9b)$$

Subsequent scans of the photoionization efficiency at m/z 40 revealed the presence of both methylacetylene[25] and allene.[38] The panel on the left hand side of Fig. 1 is a dilution study of furan pyrolysis. The 11.0 eV PIMS of furan pyrolysis at 1400 K reveals the presence of m/z 15 at 0.15% furan/He dilutions, but as the dilution increases to 0.04%, 0.015%, and to 0.0075%, m/z 15 vanishes while strong signals at m/z 39, 40, and 42 persist. Other products of bimolecular chemistry, HCC-CCH (m/z 50), HCC-CH=CH_2 (m/z 52), and C_6H_6 (m/z 78) also disappear upon dilution of the furan sample.

The right-hand panel of Fig. 1 clearly demonstrates that the thermal cracking of furan diluted to 0.01% in He follows the predictions of Scheme I. PIMS at 11.7 eV of pyrolysis of furan-d_0 at 1400 K produces $HCCH^+$ (m/z 26), $HCCCH_2^+$ (m/z 39), HCC-CH_3^+ (m/z 40), and $CH_2{=}C{=}O^+$ (m/z 42). The parent species furan (m/z 68) is almost completely consumed. A concentration of 0.01% furan was chosen to minimize bimolecular chemistry and was adopted as the operating condition for the remainder of experiments.

The pyrolysis of 0.01% furan/He with 10.4 eV PIMS detection of the products as a function of temperature is shown in Fig. 2. With the μtubular reactor at 300 K, only signals for furan (m/z 68) and the mono-^{13}C isotope peak (m/z 69) are observed; there are trace signals around m/z 50 due to an unknown cause. As the reactant gas is heated to temperatures between 1000 K and 1100 K,

furan decomposition begins. Signals for CH_3CCH (m/z 40) and CH_2CO (m/z 42) are clearly observed. Heating the gas mixture to 1300 K leads to the production of the propargyl radical at m/z 39. The highest temperature recorded is 1400 K and Fig. 2 shows that the consumption of furan (m/z 68) is nearly complete.

Fig. 3 is a set of PIE curves at m/z 39 that unambiguously identifies propargyl radical as a thermal cracking product of furan. At temperatures of 1200 K, there are only faint signals at m/z 39 (open, black trace), but upon heating the gas mixture to 1400 K, the PIE curve at m/z 39 (solid, red trace) is observed. The origin is observed at 8.7 eV, the known threshold for propargyl radical.[24] The measured PIE curve for propargyl radical[29] is plotted in the solid, black scan and matches the PIE(m/z 39) resulting from furan pyrolysis until about 10 eV.

In addition to furan-d_0, its isotopomer furan-d_4 was also thermally decomposed. When pyrolysis is carried out of a 0.01% mixture of furan-d_4/He, PIE curves and PIMS at 11.7 eV detects the expected species: $DCCD^+$ (m/z 28), $DCCCD_2^+$ (m/z 42), $DC{\equiv}CCD_3^+$ (m/z 44), and $CD_2{=}C{=}O^+$ (m/z 44). When a cross-over experiment of a 0.01% diluted 1:1 mixture of [furan-d_0:furan-d_4] is pyrolyzed, no mixed products are observed. PIMS only detects: [$HCCH^+$ (m/z 26), $HCCCH_2^+$ (m/z 39), $HC{\equiv}CCH_3^+$ (m/z 40), and $CH_2{=}C{=}O^+$ (m/z 42)] as well as [$DCCD^+$ (m/z 28), $DCCCD_2^+$ (m/z 42), $DCC\text{-}CD_3^+$ (m/z 44), and $CD_2{=}C{=}O^+$

(m/z 44)]. All of this suggests that only unimolecular decomposition is observed at this concentration of furan.

Figs. 1, 2, and 3 confirm the predictions of Scheme I. PIMS below 12 eV detects $HCCH^+$ (m/z 26), $HCCCH_2^+$ (m/z 39), $HC{\equiv}CCH_3^+$ (m/z 40), CH_2CO^+ (m/z 42), and furan (m/z 68) but not H^+ atoms[39] or carbon monoxide.[22] The pyrolysis of furan in a hot, continuous flow SiC μtubular reactor is in agreement with interpretations based on the earlier shock tube measurements[14,16] and the pulsed μtubular reactor findings[19]; moreover the present results are consistent with theoretical predictions.[18]

b) Measurement of the Ketene/Acetylene Ratio

The mechanism in Scheme I predicts that the ratio of ketene to acetylene will be unity. Application of eq. (6) to measure the ketene/acetylene ratio yields expression (10).

$$\frac{[CH_2CO]}{[HCCH]} = \frac{S_{42}^+}{S_{26}^+}\left[\frac{\sqrt{26}\ \Phi_{HCCH}\sigma_{HCCH}}{\sqrt{42}\ \Phi_{CH_2CO}\sigma_{CH_2CO}}\right] \tag{10}$$

When photoionization measurements of CH_2CO and HCCH are carried out in at the same energy, the photon flux Φ(E) cancels in eq. (10):

$$\frac{[CH_2CO]}{[HCCH]} = \frac{S_{42}^+}{S_{26}^+}\left[\frac{\sqrt{26}\ \sigma_{HCCH}}{\sqrt{42}\ \sigma_{CH_2CO}}\right] \tag{11}$$

Fig. 4 is a plot of the measured photoionization cross sections for carbon monoxide,[28] acetylene,[21] propargyl radical,[29] methylacetylene,[30] ketene,[31] and furan.[31] The cross sections for ketene and acetylene only overlap in a small window, 11.4–11.7 eV. However, at these energies, the parent furan dissociatively ionizes to produce CH_2CO^+ and other daughter ions

$$\text{Furan}^* + \hbar\omega_{11.7\text{eV}} \rightarrow (\text{Furan}^*)^+ \rightarrow CH_2CO^+ \tag{12}$$

which greatly complicates the effort to estimate the ratio of acetylene to ketene *produced by the pyrolysis.* Consequently, two different photon energies were chosen for this estimate: 10.4 or 10.5 eV for ketene, and 11.7 eV for acetylene. The results of the calculations shown in Fig. 5 (open red trace for 10.4 eV ionization of CH_2CO, solid black trace for 10.5 eV) indicate an approximate temperature independence, however, as a group they fall quite a bit below the expected ratio of unity. These calculations, however, require knowledge of the photon fluxes Φ(10.4 eV), Φ(10.5 eV) and Φ(11.7 eV), which are based on the current measured with a photodiode and a manufacturer's calibration. However, an empirical finding in this work is that the photon fluxes at energies above *ca.* 10-11 eV are considerably underestimated by the diode measurement. In addition to the previously noted qualitative difference between the propargyl PIE curve and measured cross sections above 10 eV, a similar discrepancy was found for the PIE curve of room temperature furan. Whether this is a problem with the photodiode calibration or an unknown instrumental issue, it seems logical to

attribute the "low" $\left[\frac{[CH_2CO]}{[HCCH]}\right]_T$ ratios determined above to this effect; acetylene was measured at a higher photon energy, where the photon flux is apparently underestimated. Consequently, the concentration of acetylene is overestimated by the same proportion. This finding of "excess" HC≡CH, being consistent with the observed differences between PIEs measured in this work and those constructed from experimental cross-section data, reinforces the view that quantitative measurements of this sort must be done at the same, or very similar, photon energies to be reliable.

Fortunately, the problems above could be circumvented at the highest temperature: 1400 K, where – as noted before – the destruction of the furan precursor is nearly complete. Accordingly, the ketene ions produced by dissociative ionization of furan are not present, and one can then use a higher photoionization energy for CH_2CO. Using 11.6 and 11.7 eV photons to ionize both acetylene and ketene, the photon flux contribution to eq. (10) cancels, and the results obtained are shown in Fig. 5 with solid red and open black circles, respectively. With the common photon energy measurements, which should be regarded as *the only reliable* absolute estimates available here for the reasons discussed above, the ratio is effectively unity, as expected from the chemical mechanism in Scheme I. However, in the other measurements where different photon energies were used, the errors due to the photon flux measurement are constant and presumably independent of temperature, so that the corresponding

data in Fig. 5 should deviate from the actual ratios by a simple scaling factor. The fact that the different photon energy procedure produces a value of $\left[\frac{[CH_2CO]}{[HCCH]}\right]_T$ about 60% of that obtained in the common photon energy measurement at 1400 K means that all of the results obtained with the former procedure should be scaled by a factor of roughly $(0.6)^{-1}$ or 1.6. Thus, all measurements over the temperature range of 1100–1400 K can be seen to be consistent with the mechanism in Scheme 1.

Finally, the uncertainties for the $\frac{[CH_2CO]}{[HCCH]}$ ratio at common photon energies of 11.6 and 11.7 eV are determined by propagating the uncertainty associated with each molecule's photoionization cross-section, the measured signal and the mass discrimination factor. The uncertainty associated with the photoionization cross-section of ketene[31] at 11.6 and 11.7 eV is estimated to be 0.8 Mb and 0.5 Mb, respectively while the uncertainty for acetylene[21] is about 1 Mb at these energies. The measured signal is calculated by a summation of the ion counts over a given mass range, following a Poisson process that results in random variations in the signal. The relative uncertainty associated with this random variation is estimated to be $\sqrt{S_i}/S_i$, where S_i is the observed signal. The larger the signal-to-noise ratio for a given ion peak, the less uncertainty there is with the signal as measured. The mass discrimination factor, D_i, has been estimated to be $\sqrt{m_i}$. Since only ratios are considered for this work and not

absolute number densities, the level of uncertainty with respect to the uncertainty of the mass discrimination factor is reduced for similar masses.

b) Measurement of the [α-Carbene]/[β-Carbene] Ratio

Fig. 2 demonstrates that thermal decomposition of furan begins as the reactant mixture is heated to 1000–1100 K (corresponding to SiC wall temperatures of 1200–1300 K) and the appearance of $CH_3C{\equiv}CH^+$ (m/z 40) and $CH_2{=}C{=}O^+$ (m/z 42) is observed. In Scheme I, ketene is shown as a product of the decomposition of the α-carbene while methylacetylene results from the β-carbene. The temperature-dependent PIMS in Fig. 2 suggest that the branching ratio of products resulting from these two channels is changing as the reactant mixture is heated from 1100 K to 1400 K. From Scheme I, it is predicted that the $[\alpha/\beta]_T$ ratio could be measured in a variety of ways as indicated in eq. (3). Taking the ionization energies and cross-sections (see Fig. 4) into account, the following approaches can be used to estimate this ratio experimentally:

$$\left[\frac{\alpha-\text{carbene}}{\beta-\text{carbene}}\right] = \frac{[\text{CH}_2\text{CO @ 10.4 eV}]}{[\text{HCCCH}_2\text{@ 10.4 eV}] + [\text{HCCCH}_3\text{@ 10.4 eV}]} \tag{13a}$$

$$\left[\frac{\alpha-\text{carbene}}{\beta-\text{carbene}}\right] = \frac{[\text{CH}_2\text{CO @ 10.5 eV}]}{[\text{HCCCH}_2\text{@ 10.5 eV}] + [\text{HCCCH}_3\text{@ 10.5 eV}]} \tag{13b}$$

$$\left[\frac{\alpha-\text{carbene}}{\beta-\text{carbene}}\right] = \frac{[\text{HCCH @ 11.7 eV}]}{[\text{HCCCH}_2\text{@ 10.4 eV}] + [\text{HCCCH}_3\text{@ 10.4 eV}]} \tag{13c}$$

$$\left[\frac{\alpha-\text{carbene}}{\beta-\text{carbene}}\right] = \frac{[\text{HCCH @ 13.6 eV}]}{[\text{CO @ 14.0 eV}]} = \frac{S^{+}_{26}}{S^{+}_{28}}\ \frac{\sqrt{28}}{\sqrt{26}}\ \frac{\Phi(14.0\text{ eV})\sigma_{\text{CO}}}{\Phi(13.6\text{ eV})\sigma_{\text{HCCH}}} \tag{13d}$$

These relationships (13a – 13d) have been used in the construction of Fig. 6. The first two measurements are carried out at a common photon energy, which as elaborated upon in Section IV.b, is the preferred route; the other two latter estimates require detailed considerations described below. Also included for comparison is the curve fit from Fulle *et al.*[16] who measured the $\left[\frac{[\text{HCCH}]}{[\text{CO}]}\right]_{\text{T}}$ ratio in a shock tube, quantifying these species using electron impact, time-of-flight mass spectrometry.

First, when the $\left[\frac{\alpha-\text{carbene}}{\beta-\text{carbene}}\right]_{\text{T}}$ ratio is determined from eqs. (13a) and (13b) – those using a common photon energy – the results agree very well with each other and exhibit a smooth behavior of the ratio as a function of the reciprocal temperature. The temperature-dependence of these results is qualitatively consistent with those of Fulle *et al.*,[16] although the magnitude of the ratios measured here is only about 50% that found in the shock-tube study. Nevertheless, these two measurements, representing independent determinations of the ratio under conditions that avoid the photon flux issue mentioned earlier, give very similar results, which is suggestive that the ratios produced in our experiments are smaller than those reported by Fulle *et al.*

Turning now to the measurements of the ratio that (necessarily) are based on measurements at different photon energies, the determination of eq. (13c) is based on the signal of HCCH and the total measured signal of [$HCCCH_2$] and [$HCC\text{-}CH_3$]. An expedient workaround for determining this ratio is to use the same photon energies used to estimate the acetylene:ketene ratio (10.4 or 10.5 eV *vs.* 11.7 eV) in Section IV.b and use the lower photon energy also for methylacetylene. This introduces the same systematic error into the determination of the ratio in eq. (13c) as in the determination in eq. (10). Consequently, the $\frac{[HCCH]}{[HCCCH_2]+[HCCCH_3]}$ ratio in Fig. 6 has been corrected for the average observed shift in the $\left[\frac{CH_2CO}{HCCH}\right]_T$ ratio, as shown in Fig. 5 and discussed earlier. When this empirical correction is applied, the curves are similar to those taken at the same photon energy, providing further evidence in our finding that the ratio of the α-carbene to the β-carbene channels varies from about 15% at 1100 K to about 25% at 1400 K.

Determination based on eq. (13d) uses a smaller difference in photon energies than that in eq. (13c), however it requires other considerations. Specifically, we know there are small interfering signals at m/z 28 due to N_2^+ that results from photoionization of background air in the chamber by residual, higher VUV harmonics that are not filtered out from the synchrotron. In addition, at these high temperatures, CO can be produced from wall reactions of

the SiC μtubular reactor by oxygen impurities, and production of CO by other mechanisms (dissociative photoionization) at such high energies is another possibility. Taken together, it is then perhaps not so surprising that the $\left[\frac{[HCCH]}{[CO]}\right]_T$ ratio estimated from eq. (13d) and plotted as (□), does not display a smooth downward trend as a function of T^{-1}. Nevertheless, the ratio determined here is low – as might be expected because of both the extra sources of CO mentioned above and the higher photon energy used to measure it – but not entirely incongruent with the preferred determinations by eqs. (13a) and (13b), as well as the empirically adjusted ratios based on eq. (13c).

The uncertainty limits indicated in Fig. 6 have been determined by propagating the uncertainty associated with each of the components required for calculating the ratios, considering the photoionization cross-section, $\sigma_i(E_j)$, the measured signal, S_i^+, and the mass discrimination factor, D_i, as described for the ketene to acetylene ratio in Section IV.b. In addition to these components, there is uncertainty associated with correcting for the photon flux from 13.6 eV to 14.0 eV for the acetylene to carbon monoxide measurement. Since this is a small photon energy difference, the photocurrent correction based on the photodiode measurement of $\Phi(E)$ is estimated to induce an additional 10% relative uncertainty. Within the measurement of carbon monoxide there is also a large uncertainty due to the measured signal at m/z 28 (N_2^+ and CO^+ from wall reactions) which is difficult to estimate. However, it should be noted that both of

these sources of uncertainty are largely systematic (underestimation of photon flux at higher energies and "background" signals at m/z 28, which suggests that the data points from eq. (13d) are systematically too low.

c) Measurement of the [Propargyl Radical]/[Methylacetylene] Ratio

Scheme I predicts that both HCC-CH_3 and $HCCCH_2$ result from the favored β-carbene fragmentation mechanism. A radical channel to form $HCCCH_2$, CO, and H is observed at the higher temperatures in Fig. 2. We intend to measure the $\frac{[HCCCH_2]}{[HCC\text{-}CH_3]}$ ratio by use of eq. (8). It would behoove us to use a common photon energy to photoionize both propargyl radical and methylacetylene, in which case eq. (8) simplifies to eq. (14).

$$\frac{[HCCCH_2]}{[HCC\text{-}CH_3]} = \frac{S_{39}^{+}}{S_{40}^{+}}\left[\frac{\sqrt{40}\,\sigma_{HCC\text{-}CH_3}}{\sqrt{39}\,\sigma_{HCCCH_2}}\right]. \tag{14}$$

However Fig. 4 indicates that the overlap of $\sigma_{HCCCH2}(E)$ and $\sigma_{HCC\text{-}CH3}(E)$ is the small energy window of 10.4 – 10.5 eV. This is unfortunate, because m/z 39 is observed in photoionization of rotationally/vibrationally excited methylacetylene in this energy range, which is most likely arising from dissociative photoionization of $[CH_3C{\equiv}CH]^*$. An adjustment for methylacetylene dissociative ionization was approximated by heating $CH_3C{\equiv}CH$ over the temperature range of 1300 K – 1600 K and measuring the m/z 39 ion signal relative to that of the m/z 40. It is estimated that 6% of observed CH_3CCH^+ will

fragment to give m/z 39 at 1400 K and 3% at 1300 K. And it should be remembered in the evaluation of eq. (14) that the photoionization cross-sections of both molecules in their ground state, $\sigma_{PIMS}(HC{\equiv}CCH_3)$ and $\sigma_{PIMS}(HCCCH_2)$, may be quite different than that for the rotationally/vibrationally excited species, $\sigma_{PIMS}(HC{\equiv}CCH_3^*)$ or $\sigma_{PIMS}(HCCCH_2^*)$. For example, ionization of $HC{\equiv}CCH_3$ is a decidedly non-vertical process[40] and the dependence of cross section on photon energy will consequently be sensitive to vibrational excitation.

Fig. 7 is a plot of $\frac{[HCCCH_2]}{[HCC\text{-}CH_3]}$ over the range of 1100 K – 1400 K. The ratio was computed from eq. (14) using the experimental photoionization cross sections for propargyl radical[29] and methylacetylene.[30] The solid data points result from photoionization at 10.4 eV while those in the open circles result from photoionization at 10.5 eV. The two data sets are shifted slightly to reveal different error bars. At the lower temperatures, 1100 K – 1300 K, there are no propargyl radicals present and only $HCC\text{-}CH_3$ is detected from the β-carbene channel. As the μtubular reactor is heated, the fraction $\frac{[HCCCH_2]}{[HCC\text{-}CH_3]}$ rises from roughly 2% (1300 K) to about 10% (1400 K).

The uncertainty limits included in Fig. 7 have been determined by propagating the uncertainty associated with each of the components required for calculating the ratios, considering the photoionization cross-section, $\sigma_i(E)$, the measured signal, S_i^+, and the mass discrimination factor, D_i. As indicated above,

there is a large uncertainty associated with dissociative ionization of methylacetylene to m/z 39. In order to make an accurate estimate of the radical channel to the closed shell channel, the signal of m/z 39 should be analyzed at a lower energy, around 9 eV, and methylacetylene at 10.4 eV. However when analyzing over this large energy range we encounter the problems associated with uncertainty in the photocurrent measured by the photodiode as elaborated upon throughout this section.

V. Conclusions

Figs. 1, 2, and 3 effectively summarize the results of experiments on the pyrolysis of furan that were carried out in a CW SiC μtubular reactor. These findings act to confirm the earlier results[19] for furan pyrolysis in a pulsed SiC reactor that used both He and Ar buffer gases. The initial steps in the pyrolysis are shown in Scheme I, which provides a general chemical mechanism for this important process.

The branching ratio of the α-carbene relative to that of the β-carbene in Scheme I is important. At the lowest elevated temperature studied (1000 K), there are clearly products from both channels. A weak temperature dependence is observed, which is qualitatively consistent with that found by a shock-tube study fifteen years ago[16] under slightly different reaction conditions. While the absolute ratios found here by four different approaches are in quite good mutual agreement, they are about a factor of two smaller than those found in Fulle *et*

al.[16]. At the lowest temperatures that we study (1000 K – 1100 K), roughly 85% of the reaction goes through the β-carbene. Heating the reactant gas in the SiC μtubular reactor to 1400 K increases the flux *via* the α-carbene to about 25%. While the shock-tube findings of Fulle *et al.* predict that more reactive flux goes through the α-carbene, both studies agree that the β-carbene channel is favored.

Figure 7 shows that as reaction proceeds through the β-carbene channel, the intermediate, CH_2=C=CH-CHO, mostly rearranges to HC≡CCH_3 + CO and very little fragments to H + CO + $HCCCH_2$. Indeed, below 1300 K there are no $HCCCH_2$ radicals detected. As the chemical temperature approaches 1400 K, roughly 10% of the products from β-carbene channel crack to radicals.

This study shows the degree to which the μtubular reactor can be used to study high-temperature pyrolysis. In addition to the valuable qualitative information provided in these studies (speciation), the present work has shown that quantitative information (branching ratios) can be determined with synchrotron radiation PIMS. It is encouraging here that two independent measures of the α-carbene to β-carbene branching ratio that used common photon energies (thereby avoiding the issues with the photon flux measurements) gave nearly identical results. Although practical problems associated with dissociative photoionization, cross-section dependence on temperature, *etc.* remain with such analysis, the major issue at present with quantitative determination using the μtubular reactor is that the reactor

temperature is not well-characterized beyond wall temperature measurements, an issue that warrants attention and future study.

Acknowledgments: We would like to acknowledge support from the United States Department of Energy (grant: DE-FG02-93ER14364), the United States Department of Energy's Office of the Biomass Program (Contract no. 1544759) and the National Science Foundation (CHE-0848606 and CHE-1112466) for JWD, JFS, and GBE. MA and AG and are supported by the Director, Office of Energy Research, Office of Basic Energy Sciences, and Chemical Sciences Division of the U.S. Department of Energy under contracts No. DE-AC02-05CH11231. JFS also acknowledges support from the Robert A. Welch Foundation (Grant F-1283) and the United States Department of Energy, Basic Energy Sciences (DE-FG02-07ER15884). MRN is supported by United States Department of Energy's Bioenergy Technology Office, under Contract No. DE-AC36-99GO10337 with the National Renewable Energy Laboratory.

References

[1] Y. Román-Leshkov, C. J. Barrett, Z. Y. Liu, and J. A. Dumesic, Nature **447**, 982-5 (2007).

[2] J. B. Binder and R. T. Raines, J. Am. Chem. Soc. **131**, 1979-85 (2009).

[3] M. S. Mettler, D. G. Vlachos, and P. J. Dauenhauer, Energy Env. Sci. **5**, 7797-809 (2012).

[4] C. L. Yaws, *Yaws' Handbook of Thermodynamic and Physical Properties of Chemical Compounds*. (Knovel, New York 2011).

[5] E. Christensen, J. Yanowitz, M. Ratcliff, and R. L. McCormick, Energy & Fuels **25**, 4723-33 (2011). The molar blending research octane number (RON) and motor octane number (MON) have been calculated. RON(2-methylfuran) = 131 and MON(2-methylfuran) = 101; RON(2, 5-dimethylfuran) = 137 and MON(2, 5-dimethylfuran) = 102

[6] X. S. Wu, Z. H. Huang, T. Yuan, K. W. Zhang, and L. X. Wei, Comb. and Flame **156**, 1365-76 (2009).

[7] X. S. Wu, Z. H. Huang, X. G. Wang, C. Jin, C. L. Tang, L. X. Wei, and C. K. Law, Comb. and Flame **158**, 539-46 (2011).

[8] X. S. Wu, R. Daniel, G. H. Tian, H. M. Xu, Z. H. Huang, and D. Richardson, Appl. Energy **88**, 2305-14 (2011).

[9] D. A. Rothamer and J. H. Jennings, Fuel **98**, 203-12 (2012).

[10] C. Wang, H. M. Xu, R. Daniel, A. Ghafourian, J. M. Herreros, S. Shuai, and X. Ma, Fuel **103**, 200-2011 (2013).

[11] A. Vasiliou, K. M. Piech, B. Reed, X. Zhang, M. R. Nimlos, M. Ahmed, A. Golan, O. Kostko, D. L. Osborn, K. N. Urness, D. E. David , J. W. Daily, J. F. Stanton, and G. B. Ellison, J. Chem. Phys. **137**, 164308 (2012).

[12] M. A. Grela, V. T. Amorebieta, and A. J. Colussi, J. Phys. Chem. **89**, 38-41 (1985).

[13] O. S. L. Bruinsma, P. J. J. Tromp, H. Nolting, and J. A. Moulijn, Fuel **67**, 334-40 (1988).

[14] A. Lifshitz, M. Bidani, and S. Bidani, J. Phys. Chem. **90**, 5373-7 (1986).

[15] P. P. Organ and J. C. Mackie, J. Chem. Soc. - Faraday Trans. **87**, 815-23 (1991).

[16] D. Fulle, A. Dib, J. H. Kiefer, Q. Zhang, J. Yao, and R. D. Kern, J. Phys. Chem. A **102**, 7480-6 (1998).

[17] N. R. Hore and D. K. Russell, New J. Chem. **28**, 606-13 (2004).

[18] K. Sendt, G. B. Bacskay, and J. C. Mackie, J. Phys. Chem. A **104**, 1861-75 (2000).

[19] A. Vasiliou, M. R. Nimlos, J. W. Daily, and G. B. Ellison, J. Phys. Chem. A **113**, 8540-7 (2009).

[20] W. A. Noyes Jr. and P. A. Leighton, *The Photochemistry of Gases*. (Dover Publications, New York City, 1941). Beer's Law describes the photoionization by VUV radiation of frequency, ν, traversing a gas sample a distance z, as $I(\nu) = I_o(\nu) \exp(-n\sigma(\nu)z)$. The density of the target gas is n. Since the VUV radiation is ionizing the gas, the resultant ion current, j^+, is the difference between the incident and transmitted radiation: $j^+ = (I_o - I) = I_o[1 - \exp(-n\sigma(\nu)z)]$. Because $(-n\sigma(\nu)z)$ is a small value, the photoion current can be written as $j^+ = I_o n\sigma(\nu)z$.

[21] T. A. Cool, J. Wang, K. Nakajima, C. A. Taatjes, and A. McIlroy, Int. J. Mass Spectrom. **247**, 18-27 (2005).

[22] M. Evans and C. Y. Ng, J. Chem. Phys. **111**, 8879-92 (1999). *IE*(CO) = 14.0136 ± 0.0005 eV

[23] S. T. Pratt, P. M. Dehmer, and J. L. Dehmer, J. Chem. Phys. **99**, 6233-44 (1993). *IE(*HCCH) = 91 952 ± 2 cm^{-1} (11.4006 ± 0.0002 eV)

[24] H. Gao, Y. T. Xu, L. Yang, C. S. Lam, H. L. Wang, J. A. Zhou, and C. Y. Ng, J. Chem. Phys. **135** (2011). *IE*($HCCCH_2$) = 70 156 ± 4 cm^{-1} (8.6982 ± 0.0005 eV)

[25] X. Xing, M. K. Bahng, B. Reed, C. S. Lam, K. C. Lau, and C. Y. Ng, J. Chem. Phys. **128** (2008). *IE*(CH_3CCH) = 10.36744 ± 0.00012 eV)

[26] B. H. Niu, Y. Bai, and D. A. Shirley, J. Chem. Phys. **99**, 2520-32 (1993). *IE*(CH_2CO) = 9.6191 ± 0.0004 eV

[27] G. D. Willett and T. Baer, J. Am. Chem. Soc. **102**, 6769-73 (1980). *IE*(furan) = 8.88 ± 0.01 eV

[28] J. A. R. Samson and J. L. Gardner, J. Elect. Spectro. Related Phenom. **8**, 35-44 (1976).

[29] J. D. Savee, S. Soorkia, O. Welz, T. M. Selby, C. A. Taatjes, and D. L. Osborn, J. Chem. Phys. **136**, 134307-17 (2012).

[30] T. A. Cool, K. Nakajima, T. A. Mostefaoui, F. Qi, A. McIlroy, P. R. Westmoreland, M. E. Law, L. Poisson, D. S. Peterka, and M. Ahmed, J. Chem. Phys. **119**, 8356-65 (2003).

[31] B. Yang, J. Wang, T. A. Cool, N. Hansen, S. Skeen, and D. L. Osborn, Int. J. Mass Spectrom. **309**, 118-28 (2012).

[32] T. A. Cool, K. Nakajima, C. A. Taatjes, A. McIlroy, P. R. Westmoreland, M. E. Law, and A. Morel, Proc. Comb. Inst. **30**, 1681-8 (2005).

[33] Q. Guan and J. W. Daily, **to be published** (2013).

[34] There are at least five potential sources of error for measuring the temperature of the SiC tube. (a) The inherent accuracy of the thermocouple is listed by Omega Engineering as the greater of 4.5 ºC or 1.0% from 0 — 2320 ºC. (b) Imperfect thermal contact between the thermocouple and the SiC tube. This is difficult to quantify but it is probably not the dominant factor since most of the heat transfer is expected to be by radiation, at least at higher temperatures. (c) Cooling along

the thermocouple wire away from the thermocouple junction/SiC contact point. This is probably the most important loss factor and is likely on the order of 10s ºC. (d) Extra radiative losses from the surface area added by the thermocouple. (e) The thermocouple cold junction is at the vacuum feedthrough instead of at the meter (where it would be properly compensated). The latter consideration probably contributes less than a few ºC to the error. The best way to determine the error is by experiment, either with a sample with known kinetics or by inserting a thermocouple inside the SiC tube during normal operation.

35 K. N. Urness, A. Golan, J. W. Daily, M. R. Nimlos, J. F. Stanton, M. Ahmed, and G. B. Ellison, J. Chem. Phys. **to be submitted** (2013).

36 R. S. Tranter, R. Sivaramakrishnan, N. Srinivasan, and K. Brezinsky, Int. J. Chem. Kinetics **33**, 722-31 (2001).

37 C. A. Taatjes, D. L. Osborn, T. M. Selby, G. Meloni, H. Y. Fan, and S. T. Pratt, J. Phys. Chem. A **112**, 9336-43 (2008). $\sigma(CH_3)$ at 10.471 eV = $(4.9 \pm 2.0) \times 10^{-18}$ cm^2

38 Z. Z. Yang, L. S. Wang, Y. T. Lee, D. A. Shirley, S. Y. Huang, and W. A. Lester, Chem. Phys. Lett. **171**, 9-13 (1990). $IE(CH_2{=}C{=}CH_2) = 9.6880 \pm 0.0020$ eV

39 C. E. Moore, *Atomic Energy Levels*. (Nat. Bur. Stand., Washington, DC 20402, 1971). The value listed for the ionization potential is $IE(H) = 109\,678.758 \pm 0.001$ cm^{-1} or $13.598\,437\,8 \pm 0.000\,000\,1$ eV or $313.587\,347 \pm 0.000\,001$ kcal mol^{-1}.

[40] G. Bieri, F. Burger, E. Heilbronner, and J. P. Maier, Helv. Chim. Acta **60**, 2213-33 (1977).

Figure Captions

Fig. 1 The left-hand panel demonstrates the elimination of bimolecular chemistry as shown by the disappearance of m/z 15 (CH_3) in the dilution study. Using a 0.01% furan/He mixture, secondary chemistry and the production of methyl radicals are eliminated; at 0.01% dilution there are still strong signals at m/z 39, 40, and 42. Subsequent experiments are performed at this dilution. The PIMS in the right panel is recorded at 11.7 eV and shows all primary products from furan decomposition at a chemical temperature of 1400 K: $HCCH^+$ (m/z 26), CH_3CCH^+ (m/z 40), CH_2CO^+ (m/z 42), in addition to an observed signal at m/z 39 indicating presence of propargyl radical, $HCCCH_2^+$. Based on the preliminary measurements of the "chemical temperatures" (see text), we report the effective temperature inside the reactor as [T_{wall} – 200 K]. An effective temperature of 1400 K corresponds to a measured SiC wall temperature of 1600 K. The PIMS for the dilution study at 11.0 eV sampled 5,000,000 mass spectra, compared to 100,000 for most other mass spectra, including the PIMS at 11.7 eV.

Fig. 2 The PIMS of 0.01% furan/He at 10.4 eV as a function of chemical temperature is plotted. Based on the preliminary measurements of the "chemical temperatures" (see text), we report the effective temperature inside the reactor as [T_{wall} – 200 K]. An effective temperature of 1000 K corresponds to a SiC wall temperature of 1200 K. At 1000 K, small signal of CH_3CCH^+ (m/z 40) is evident; by 1100 K methylacetylene (m/z 40) and ketene (m/z 42) are both present. At

1300 K and 1400 K the radical channel is accessible and propargyl radical (m/z 39) begins to grow in. By 1400 K nearly all of the parent furan (m/z 68) is destroyed. Pressure of the gas mixture at the reactor inlet was measured as a function of the SiC wall temperature: (T_{wall} = 1600 K, P_{inlet} = 288 Torr); (T_{wall} = 1500 K, P_{inlet} = 274 Torr); (T_{wall} = 1400 K, P_{inlet} = 256 Torr); (T_{wall} = 1300 K, P_{inlet} = 244 Torr); (T_{wall} = 1200 K, P_{inlet} = 225 Torr); and (T_{wall} = 300 K, P_{inlet} = 101 Torr).

Fig. 3 Photoionization efficiency curve of furan/He mixtures showing m/z 39 at 1400 K (●) and 1200 K (○) compared with the literature photoionization cross-section curve (●). Curve at 1400 K exhibits similar sharp features to that observed by Savee *et al.*,[29] indicative of autoionization states in the propargyl radical.

Fig. 4 The literature photoionization cross-sections used for analysis in this work are collected together in a single plot; carbon monoxide,[28] acetylene,[21] propargyl radical,[29] methylacetylene,[30] ketene,[31] and furan.[31] In order to eliminate the need for the photon flux correction term, Φ(E), the ratios were calculated in regions where the reported photoionization cross-section of one molecule of interest overlapped another molecule. The choice of an appropriate evaluating photoionization energy is critical for accurate analysis.

Fig. 5 The $\frac{[CH_2CO]}{[HCCH]}$ ratio as measured from a 0.01% furan/He mixture by PIMS at 11.6 eV (●) and 11.7 eV (○) is unity. When compared over the temperature

range 1100–1400 K, different photon energies must be used to avoid dissociative ionization. Based on the preliminary measurements of the "chemical temperatures" (see text), we report the effective temperature inside the reactor as [T_{wall} – 200 K]. The ketene/acetylene ratio as measured by CH_2CO^+ signal at 10.4 eV (○) and 10.5 eV (●) compared to $HCCH^+$ signal at 11.7 eV. The [ketene]/[acetylene] ratio is constant over the temperature range but not unity. The uncertainty in the photon flux measurements, Φ(E), is likely the cause that this ratio is less than 1.

Fig. 6 PIMS of a 0.01 % mixture of furan/He were recorded and used for a measurement of the $\left[\frac{\alpha-\text{Carbene}}{\beta-\text{Carbene}}\right]$ ratio as a function of temperature. Based on the preliminary measurements of the "chemical temperatures" (see text), we report the effective temperature inside the reactor as [T_{wall} – 200 K]. Different ratios were used to measure the $\left[\frac{\alpha}{\beta}\right]$ ratio.

$$\frac{[CH_2CO\ @\ 10.4\ eV]}{[HCCCH_2@\ 10.4\ eV] + [HCCCH_3@\ 10.4\ eV]} \quad (○),$$

$$\frac{[CH_2CO\ @\ 10.5\ eV]}{[HCCCH_2@\ 10.5\ eV] + [HCCCH_3@\ 10.5\ eV]} \quad (●),$$

$$\frac{[HCCH\ @\ 11.7\ eV]}{[HCCCH_2@\ 10.4\ eV] + [HCCCH_3@\ 10.4\ eV]} \quad (▲) \quad \text{and} \quad \frac{[HCCH\ @\ 13.6\ eV]}{[CO\ @\ 14.0\ eV]} \quad (□).$$

The results of a shock tube study[16] measuring the [HCCH]/[CO] ratio as a function of temperature are also included as a comparison.

Fig. 7 PIMS of a 0.01 % mixture of furan/He were recorded and used for a measurement of the $\frac{[HCCCH_2]}{[HCC\text{-}CH_3]}$ ratio as a function of temperature. Based on the preliminary measurements of the "chemical temperatures" (see text), we report the effective temperature inside the reactor as [T_{wall} – 200 K]. Because of small overlap of σ($HCCCH_2$) and σ($HCC\text{-}CH_3$) (Fig. 4), the propargyl radical/methylacetylene ratio was measured at 10.4 eV (●) and 10.5 eV (○).

Figures

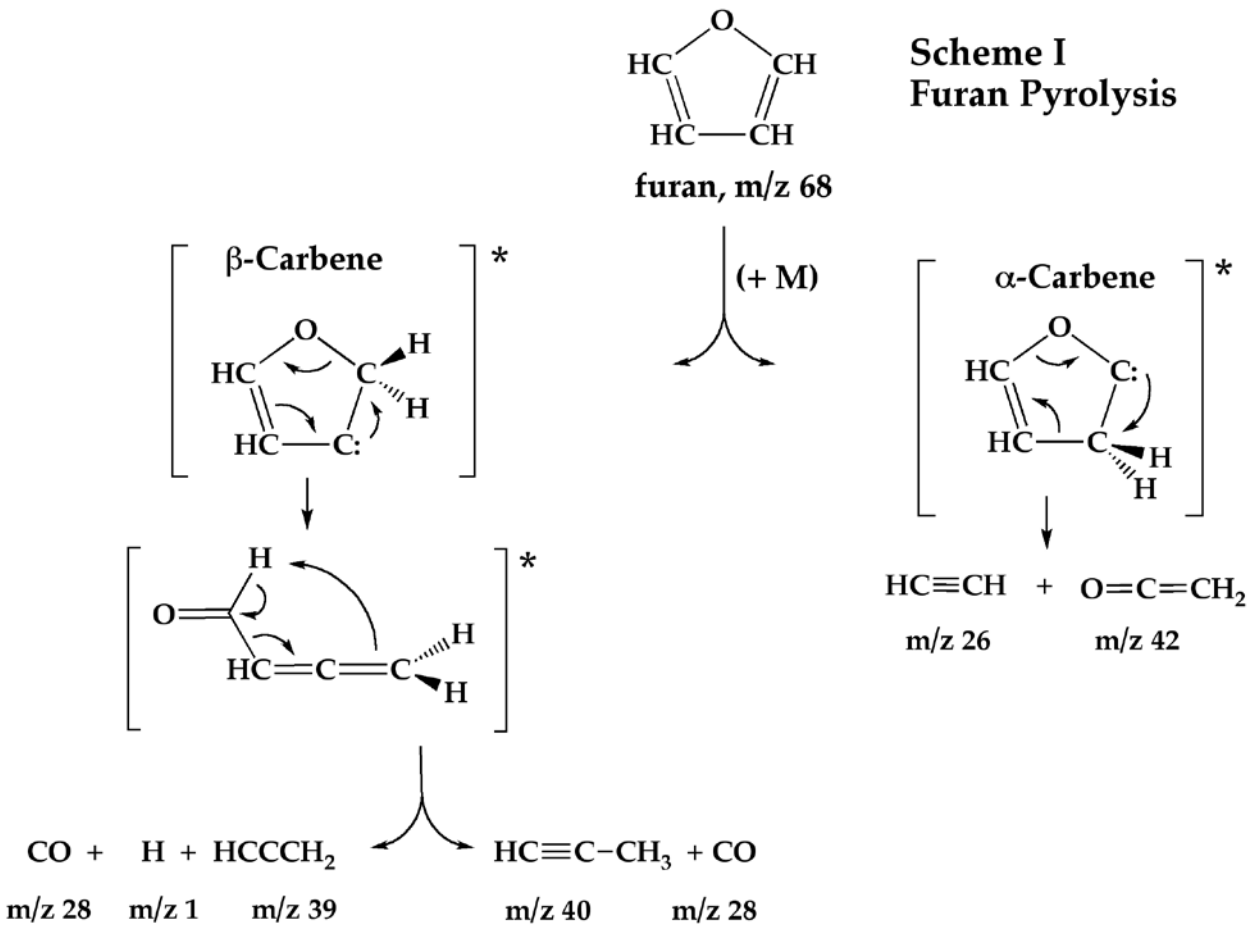
Scheme I
Furan Pyrolysis
furan, m/z 68
(+ M)
β-Carbene
α-Carbene
HC≡CH + O=C=CH2
m/z 26
m/z 42
CO + H + HCCCH2
m/z 28
m/z 1
m/z 39
HC≡C−CH3 + CO
m/z 40
m/z 28

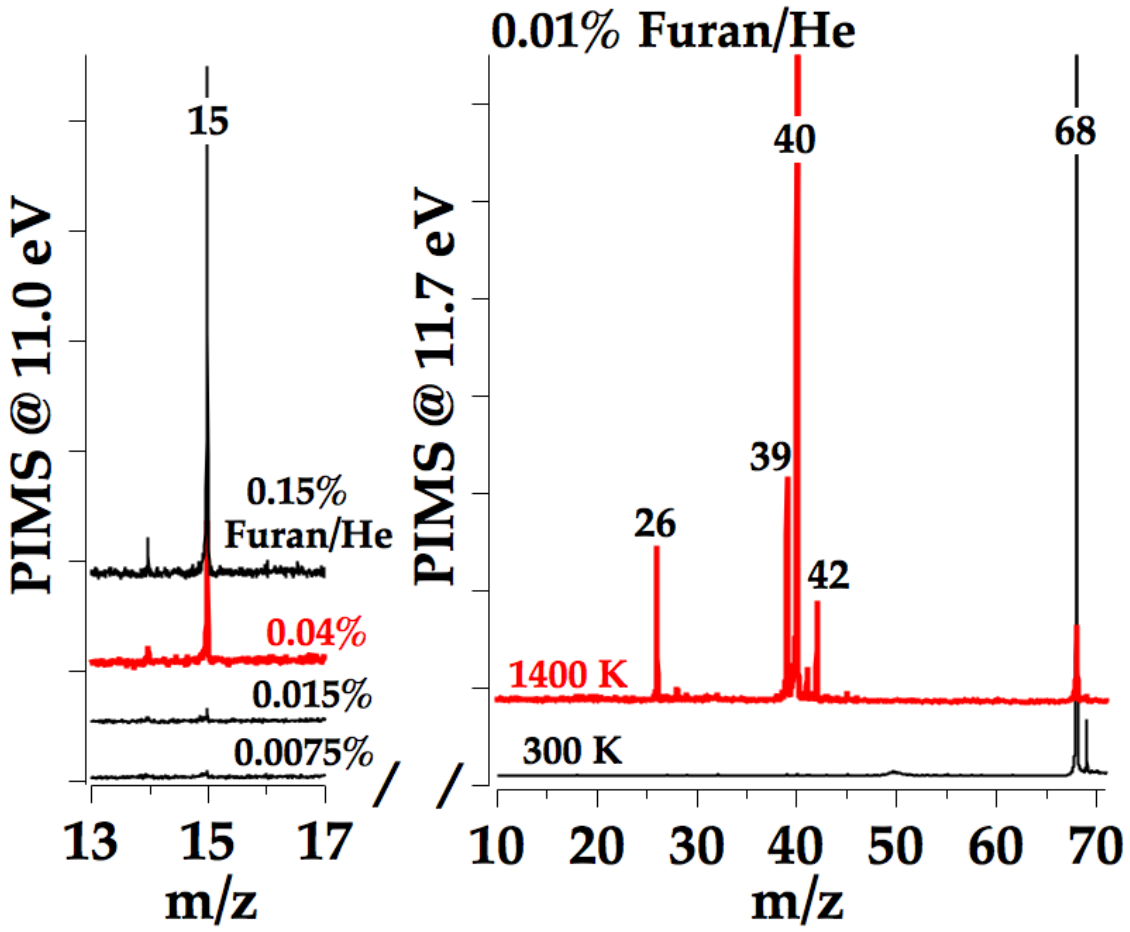
0.01% Furan/He
PIMS @ 11.0 eV
PIMS @ 11.7 eV
15
0.15%
Furan/He
0.04%
0.015%
0.0075%
40
68
39
26
42
1400 K
300 K
13
15
17
10
20
30
40
50
60
70
m/z
m/z

F1

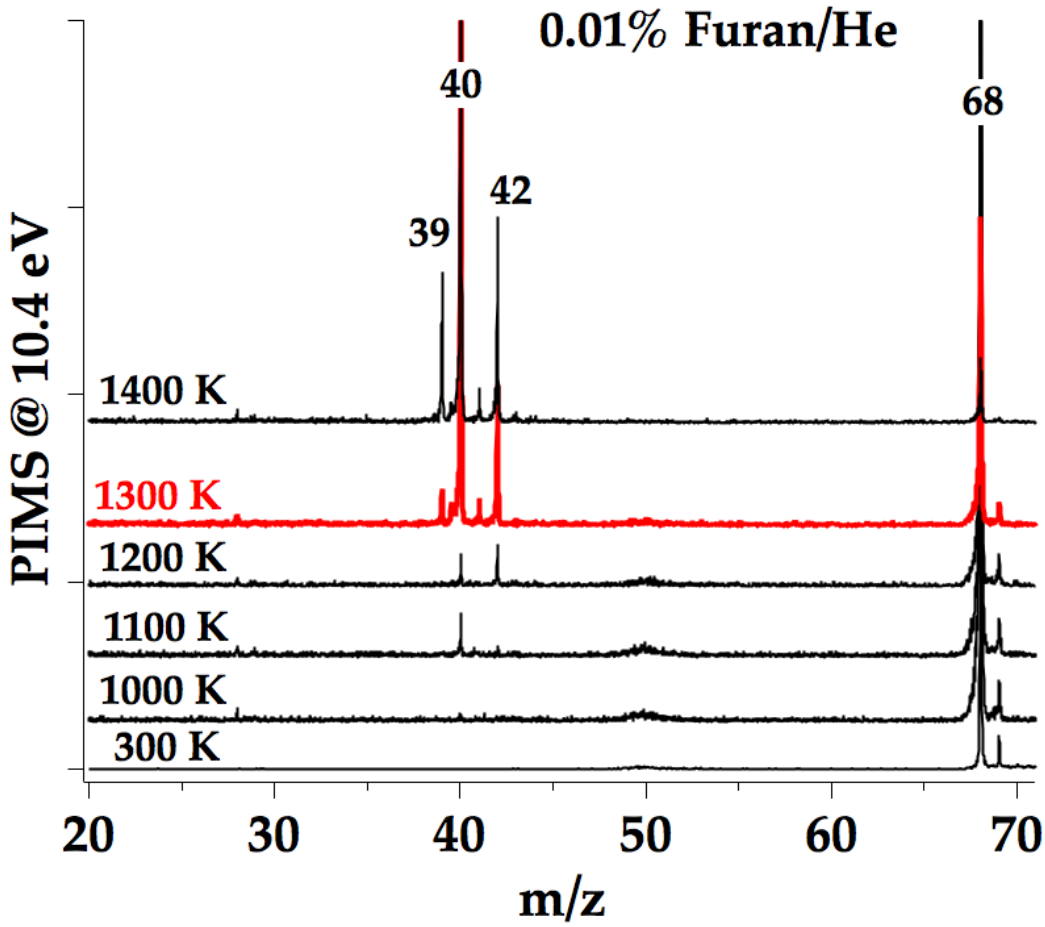
0.01% Furan/He
40
68
42
39
1400 K
1300 K
1200 K
1100 K
1000 K
300 K
PIMS @ 10.4 eV
20
30
40
50
60
70
m/z

F2

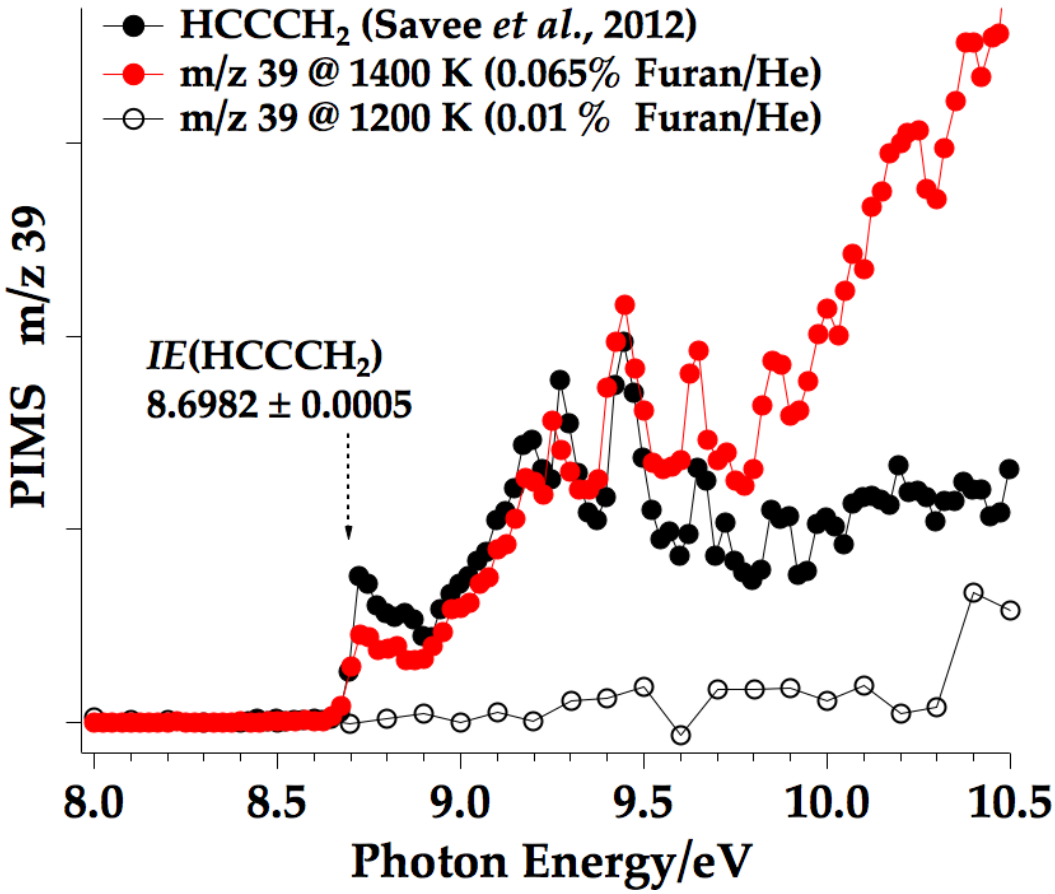
HCCCH2 (Savee et al., 2012)
m/z 39 @ 1400 K (0.065% Furan/He)
m/z 39 @ 1200 K (0.01 % Furan/He)
IE(HCCCH2)
8.6982 ± 0.0005
PIMS m/z 39
8.0
8.5
9.0
9.5
10.0
10.5
Photon Energy/eV

F3

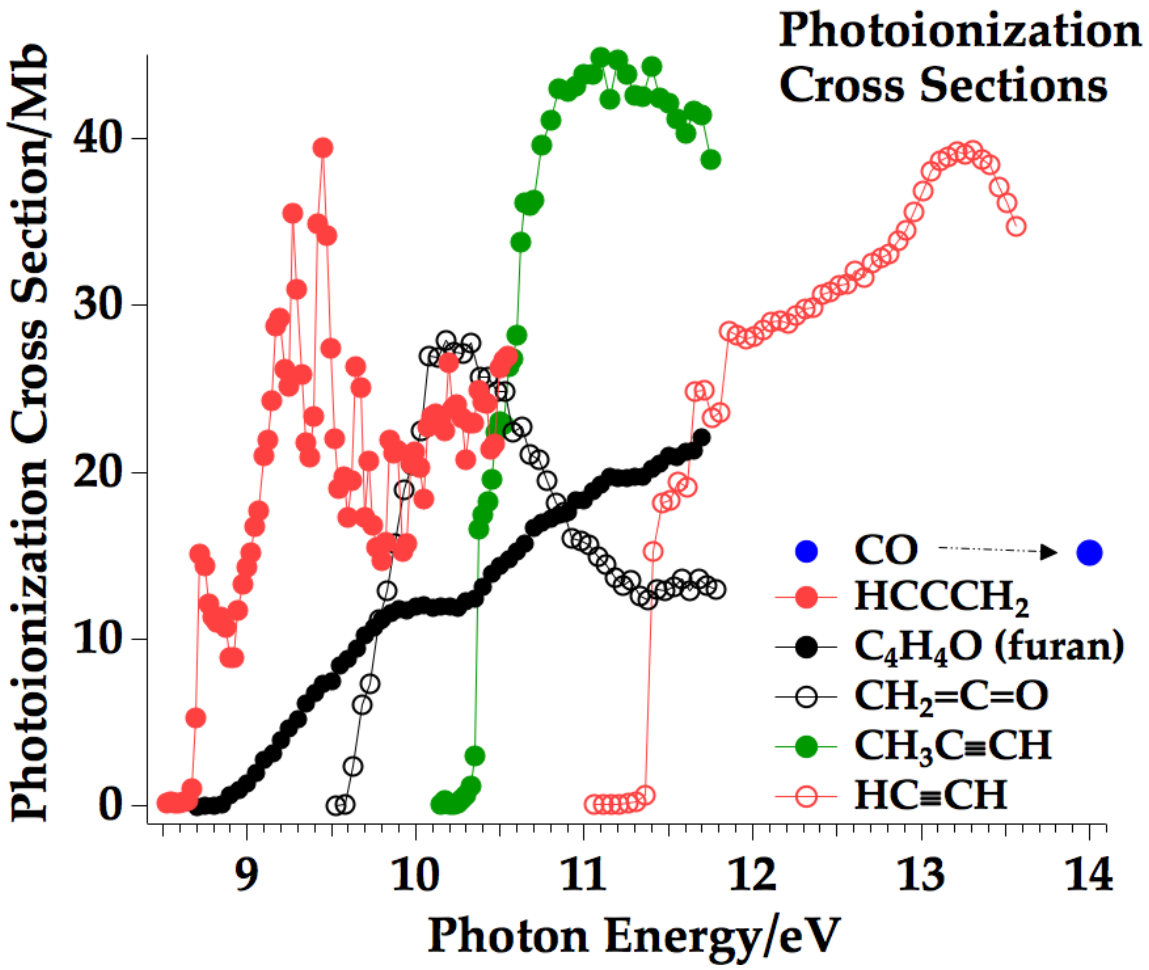
Photoionization
Cross Sections
Photoionization Cross Section/Mb
Photon Energy/eV
0
10
20
30
40
9
10
11
12
13
14
CO
HCCCH2
C4H4O (furan)
CH2=C=O
CH3C≡CH
HC≡CH

F4

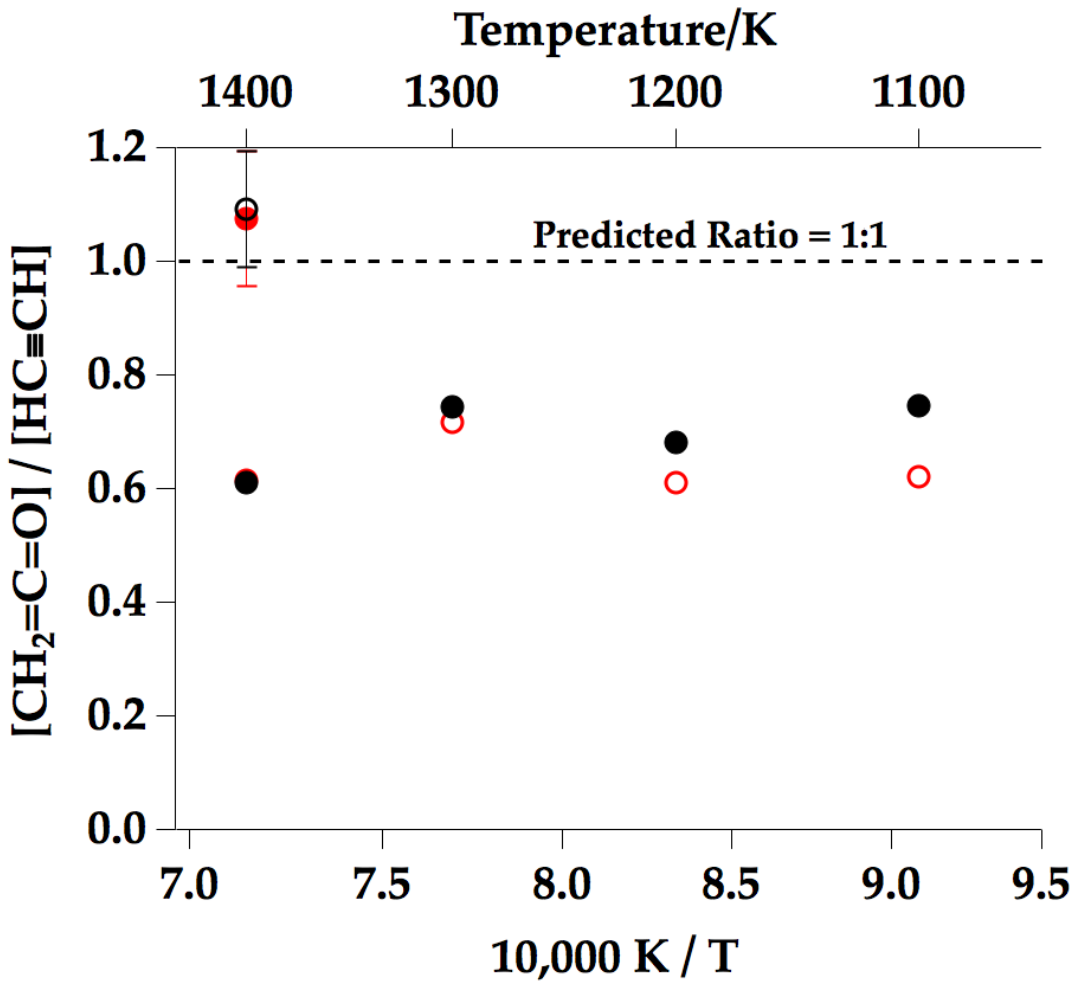
Temperature/K
1400
1300
1200
1100
1.2
1.0
0.8
0.6
0.4
0.2
0.0
Predicted Ratio = 1:1
[CH2=C=O] / [HC≡CH]
7.0
7.5
8.0
8.5
9.0
9.5
10,000 K / T

F5

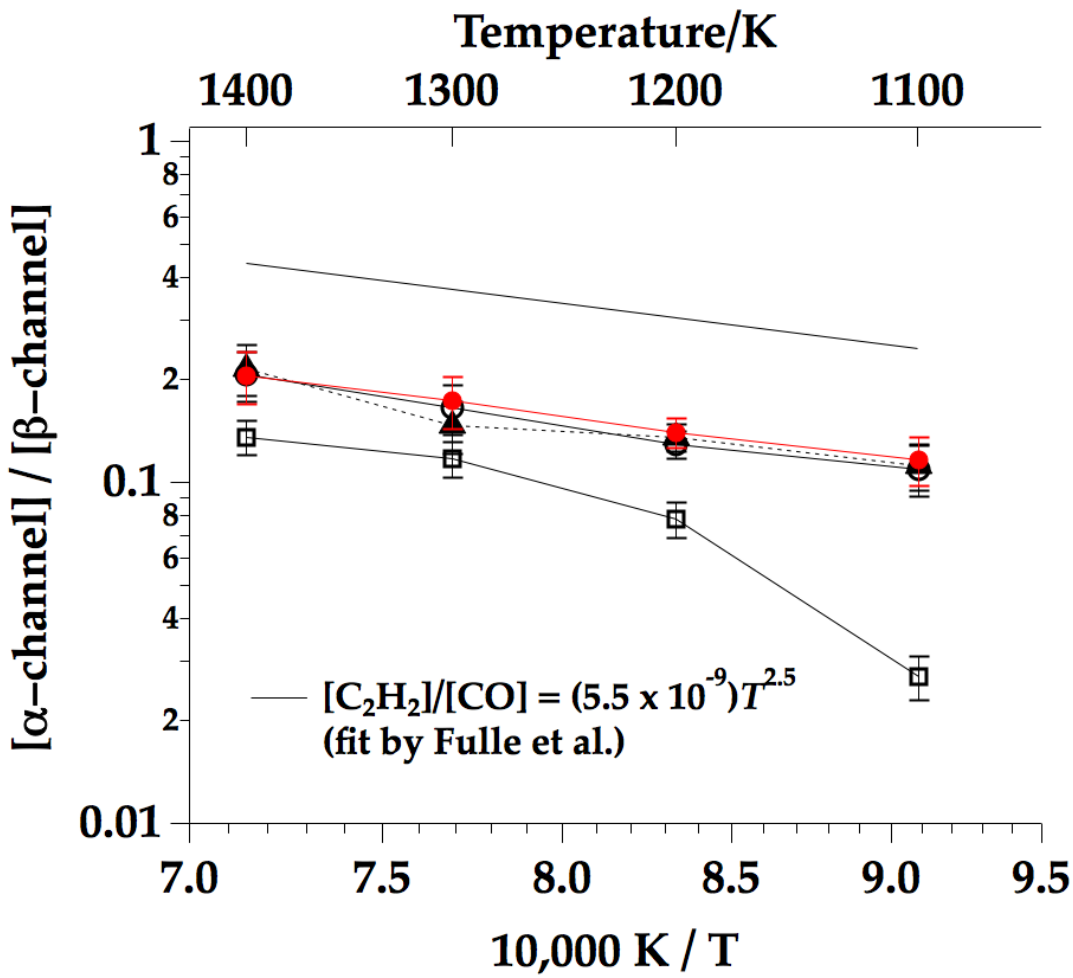
Temperature/K
1400
1300
1200
1100
1
8
6
4
2
0.1
8
6
4
2
0.01
[α−channel] / [β−channel]
[C2H2]/[CO] = (5.5 x 10-9)T2.5
(fit by Fulle et al.)
7.0
7.5
8.0
8.5
9.0
9.5
10,000 K / T

F6

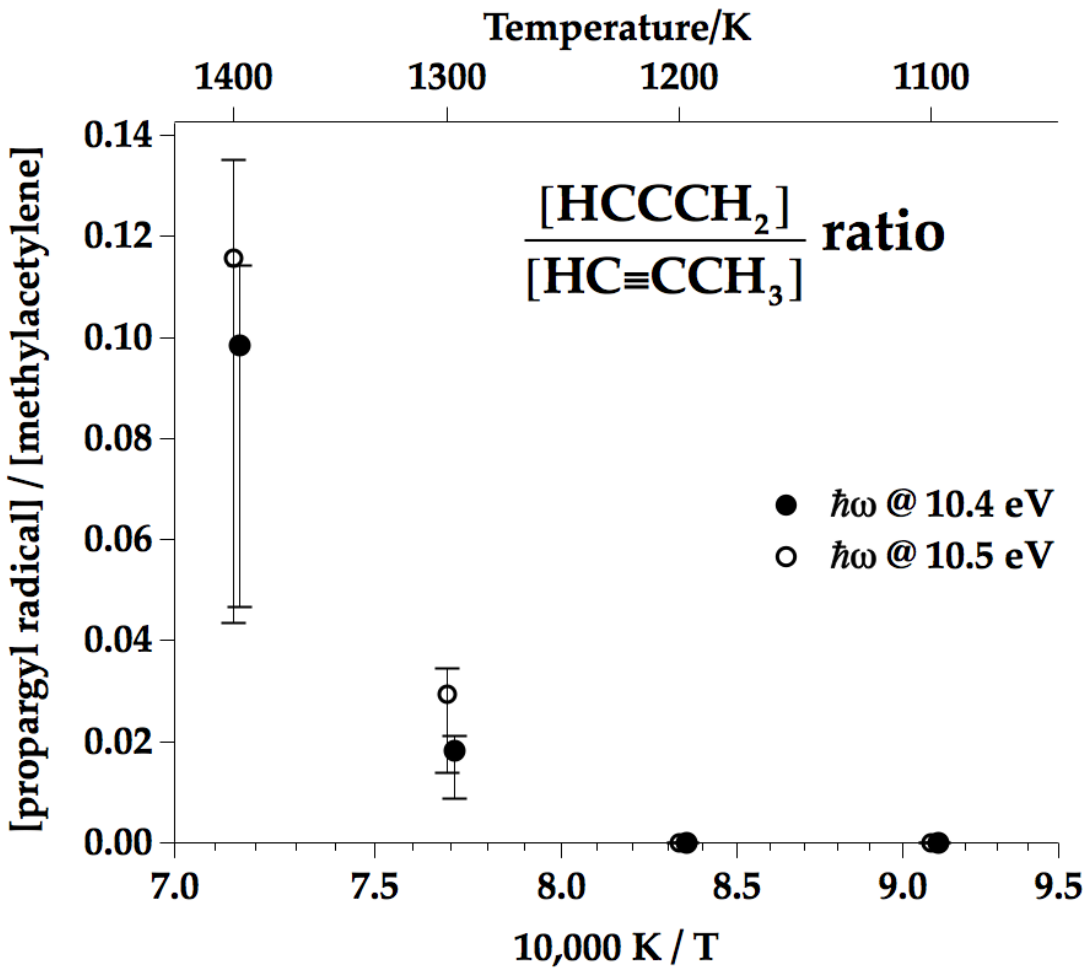
Temperature/K
1400
1300
1200
1100
0.14
0.12
0.10
0.08
0.06
0.04
0.02
0.00
[propargyl radical] / [methylacetylene]
[HCCCH2] / [HC≡CCH3] ratio
ħω @ 10.4 eV
ħω @ 10.5 eV
7.0
7.5
8.0
8.5
9.0
9.5
10,000 K / T

F7

This document was prepared as an account of work sponsored by the United States Government. While this document is believed to contain correct information, neither the United States Government nor any agency thereof, nor the Regents of the University of California, nor any of their employees, makes any warranty, express or implied, or assumes any legal responsibility for the accuracy, completeness, or usefulness of any information, apparatus, product, or process disclosed, or represents that its use would not infringe privately owned rights. Reference herein to any specific commercial product, process, or service by its trade name, trademark, manufacturer, or otherwise, does not necessarily constitute or imply its endorsement, recommendation, or favoring by the United States Government or any agency thereof, or the Regents of the University of California. The views and opinions of authors expressed herein do not necessarily state or reflect those of the United States Government or any agency thereof or the Regents of the University of California.